Crack bridging law in discontinuous fiber reinforced composites under cyclic loading

短繊維補強複合材料の繰返し載荷下ひび割れ架橋則

Takashi Matsumoto*

松本　高志

* Member, Ph.D., Assoc. Prof., Division of Built Environment, Hokkaido University (Kita-13, Nishi-8, Kita-ku, Sapporo 060-8628)

This paper presents the micromechanical modeling of fiber bridging constitutive law of a discontinuous fiber reinforced composite (DFRC) under cyclic loading. First, the derivation of fiber bridging constitutive law under monotonic loading is briefly reviewed to highlight the approach to obtain the bridging stress carried by randomly distributed discontinuous fibers. Second, the relation between single fiber pull-out/push-in load amplitude and crack opening displacement amplitude under cyclic loading is derived. Third, fiber bridging constitutive law under cyclic loading is derived and obtained in two ways: numerically and analytically. Finally, the fiber bridging constitutive law is compared with experimental data of a cyclically loaded fiber reinforced concrete (FRC), and its validity is shown.

Key Words: *Bridging law, discontinuous fiber reinforced composite, cyclic loading*

1. Introduction

Short fiber reinforced cement based composites are recently finding more applications in civil engineering. These composites exhibit superior performance in strength, ductility, and fracture toughness, when compared to conventional cementitious materials, such as mortar and concrete. These beneficial properties are exhibited due to bridging fibers that transfer stresses over cracks and resist against cracks' opening. It is known that fiber bridging constitutive law, which is the relation between bridging stress and crack opening displacement, is specific to a composite mix design, and that it governs the composite post crack behaviors[1),2)]. Therefore, the understanding of fiber bridging constitutive law is essential for developing a high performance composite that satisfies structural performance requirements.

Some of these composites' applications expect improved long-term durabilities for structures that are subjected to fatigue under traffic loading or environmental loading. Long-term durabilities can be improved with the composites' high fatigue strength, high crack resistance, and crack width control ability. For each of these properties, the understanding of fiber bridging constitutive law is again necessary. Here, in addition to the law under monotonic loading, the law under cyclic loading is required.

However, the fiber bridging constitutive law under cyclic loading has not been made available. This forces the use of fiber bridging constitutive law under monotonic loading to understand indirectly composite properties and structural performances under cyclic loading. It is necessary to develop fiber bridging constitutive law to properly treat problems under cyclic loading. Also, the fiber bridging constitutive law under cyclic loading should be based on the micromechanics of fiber bridging, being an explicit function of micromechanical parameters such as fiber length, fiber diameter, fiber modulus, fiber-matrix interfacial frictional bond strength, and so on. This is because such a micromechanics based bridging law yields understandings of mechanisms and implications of developments in an efficient way.

This paper presents the derivation of fiber bridging constitutive law of a discontinuous fiber reinforced composite (DFRC) under cyclic loading and shows the validity of the law. In chapter 2, the derivation of fiber bridging constitutive law under monotonic loading (σ_f - δ relation) is briefly reviewed to highlight the approach to obtain the bridging stress carried by randomly distributed discontinuous fibers. In chapter 3, the relation between single fiber pull-out/push-in load amplitude and crack opening displacement amplitude under cyclic loading (ΔP - $\Delta\delta$ relation) is derived. In chapter 4, fiber bridging constitutive law under cyclic loading ($\Delta\sigma_f$ - $\Delta\delta$ relation) is obtained in two

ways: numerically and analytically. Finally, in chapter 5, the theoretical $\Delta\sigma_f$ - $\Delta\delta$ relation is compared with experimental data of a cyclically loaded fiber reinforced concrete (FRC), in order to show its validity.

2. Review on Fiber Bridging Constitutive Law under Monotonic Loading

The essence of a monotonic fiber bridging constitutive law derived by Li is explained in this section[1]. The constitutive law relates the fiber bridging stress, σ_f, as a unique function of the crack opening displacement, δ, under monotonic loading. The $\sigma_f(\delta)$ has been derived based on micromechanical modeling of fiber bridging with weak (friction controlled) fiber-matrix interface. The derivation starts from constructing the relation between the fiber pull-out load, P, and the crack opening displacement, δ, of a single fiber embedded in the matrix. Then the pull-out load carried by individual fibers is integrated to construct the monotonic fiber bridging constitutive law, $\sigma_f(\delta)$.

2.1. Single Fiber Behavior under Monotonic Loading

The P - δ relation is given for two stages: debonding and sliding. The fiber pull-out behavior is summarized in the following. During debonding stage, when a single fiber embedded in the matrix is loaded for pull-out, the fiber-matrix interface undergoes debonding which extends the friction activated interfacial zone towards the embedded end of the fiber. During sliding stage, after the debonding reaches the embedded end of the embedment length, l, that is the shorter of the two on both sides of the matrix crack, the entire fiber starts sliding out of the matrix (Fig. 1).

Two assumptions are made for the derivation of the P - δ relation by Li[1]. First, an elastic fiber is assumed to be embedded in a stiff matrix. This is correct when fiber volume fraction is low and when there is a moderate contrast between fiber and matrix elastic modulus. Second, the axial strain of the
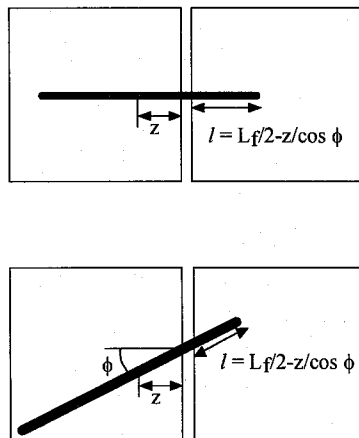
fiber is linearized by assuming that $(l / d_f)/(E_f / \tau) << 1$, where $d_f =$ fiber diameter, $E_f =$ fiber modulus, $\tau =$ interfacial frictional bond strength. This is reasonable, when (E_f / τ) is two to three orders of magnitude larger than (l / d_f). These two assumptions are reasonable for fiber reinforced cementitious materials, and the error incurred with the assumptions is reported to be less than 1 %. In the first stage during debonding, the crack opening displacement is given by stretching of the debonded portion of the embedded fiber, and the pull-out load increases with the crack opening displacement due to the extending debonded interface area. The P - δ relation is given by

$$P_d(\delta) = \frac{\pi}{2}\sqrt{E_f d_f^3 \tau \delta} \qquad for \ \delta \leq \delta_o \qquad (1)$$

where $\delta_o = (4 \ \tau \ l^2) / (E_f d_f)$ is the crack opening displacement at which debonding is completed throughout the embedment length.

In the second stage during sliding of the fully debonded fiber, the load decreases with the displacement, because the frictional interface area decreases due to the sliding-out of the fiber. The P - δ relation is given by

$$P_{sl}(\delta) = \pi\tau d_f l\left(1 - \frac{\delta - \delta_o}{l}\right) \qquad for \ \delta_o < \delta \leq l. \qquad (2)$$

The whole picture of the load-displacement relation (P - δ relation) for a single fiber with its embedment length, l, is shown in Fig. 2.

2.2. Fiber Bridging Constitutive Law under Monotonic Loading

The constitutive law is then obtained by integrating the load carried by individual bridging fibers. The integration accounts
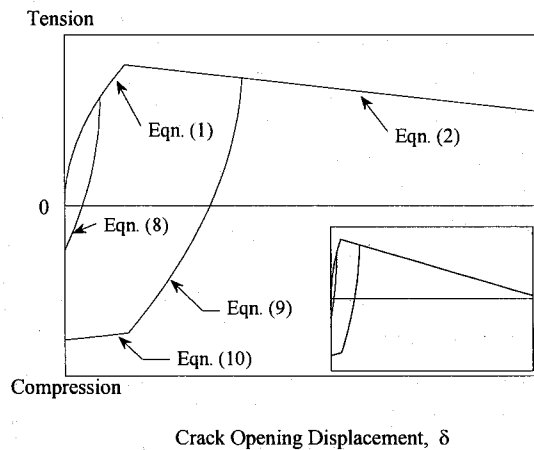

Fig. 1 Fiber centroidal distance, z, and orientation, ϕ.

Fig. 2 Single fiber loading-unloading curves with corresponding equations (insert for complete curves)[3].

for the random distribution of location and orientation of short fibers at a designated crack plane. With the assumption of 3-D uniform randomness for the fiber centroidal distance, z, and orientation, ϕ, at a designated crack plane (Fig. 1), Li derived the constitutive law for DFRCs[1]. The bridging stress, σ_f, is related to the crack opening displacement, δ, through the integration of the load carried by individual bridging fibers at different stages of debonding and sliding:

$$\tilde{\sigma}_f = \frac{8}{\pi\tau(L_f/d_f)d_f^2} \int_{\phi=0}^{\frac{\pi}{2}} \int_{z=0}^{\frac{L_f}{2}\cos\phi} P(\delta)e^{f\phi}p(\phi)p(z)dzd\phi \quad (3)$$

where $\tilde{\sigma}_f = \sigma_f/\sigma_o$, $\sigma_o = V_f \tau (L_f/d_f)/2$, $V_f =$ fiber volume fraction, $L_f =$ fiber length, $f =$ snubbing coefficient, $p(\phi) = \sin\phi$, $p(z) = 2/L_f$. The factor $e^{f\phi}$ in (3) refers to a snubbing effect which describes the mechanical interactions between a loaded inclined fiber and the matrix material[3].

Substituting (1) and (2) into (3) yields explicit equations for the constitutive law. For pre-peak bridging stress,

$$\tilde{\sigma}_f\Big|_{prepeak} = g\left[2\left(\frac{\tilde{\delta}}{\tilde{\delta}^*}\right)^{\frac{1}{2}} - \left(\frac{\tilde{\delta}}{\tilde{\delta}^*}\right)\right] \quad for \ 0 \le \tilde{\delta} \le \tilde{\delta}^* \quad (4)$$

where $g = 2/(4 + f^2)(1 + e^{\pi f/2})$, $\tilde{\delta} = \delta/(L_f/2)$, and $\tilde{\delta}^* = \delta^*/(L_f/2)$. δ^* corresponds to the maximum value of δ_o with $l = L_f/2$, at which all fibers have completed debonding. For post-peak bridging stress,

$$\tilde{\sigma}_f\Big|_{postpeak} = g\left[1 - \left(\tilde{\delta} - \tilde{\delta}^*\right)\right]^2 \quad for \ \tilde{\delta}^* < \tilde{\delta} \le 1. \quad (5)$$

The whole picture of the bridging stress-crack opening displacement relation (σ_f- δ relation) for a composite with $\tilde{\delta}^* = 0.002$ is shown in Fig. 3 and 4.

3. Single Fiber Behavior under Cyclic Loading

The cyclic fiber bridging constitutive law can be developed based on the micromechanics of fiber bridging under cyclic loading in a similar fashion as the monotonic constitutive law. The constitutive law relates the fiber bridging stress amplitude, $\Delta\sigma_f$, as a unique function of the crack opening displacement amplitude, $\Delta\delta$, under cyclic loading. The development of the cyclic fiber bridging constitutive law will start again from constructing the relation between the pull-out/push-in load amplitude, ΔP, and the crack opening displacement amplitude, $\Delta\delta$, of a single fiber embedded in the matrix. Then the pull-out/push-in load amplitude carried by individual fibers is integrated to construct the cyclic fiber bridging constitutive law, $\Delta\sigma_f(\Delta\delta)$.
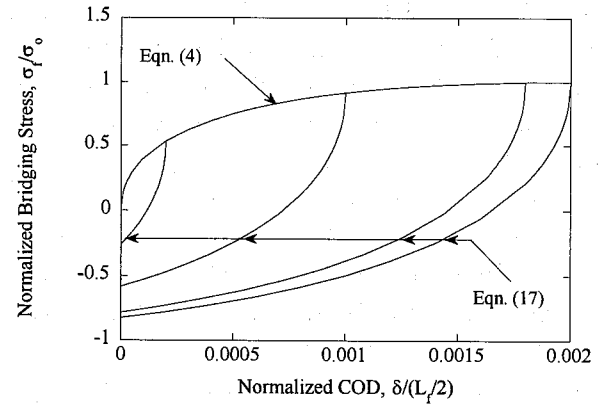

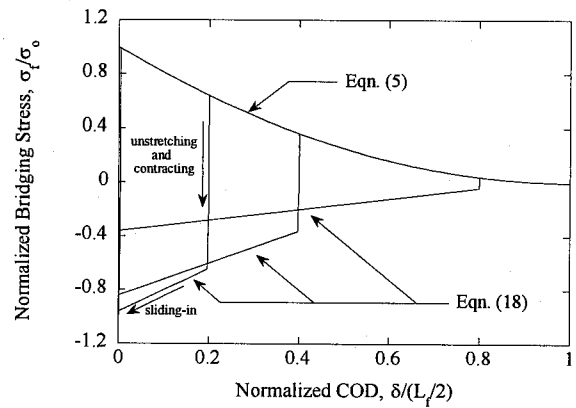Fig. 3 Loading-unloading curves for pre-peak bridging stress[3].

Fig. 4 Loading-unloading curves for post-peak bridging stress[3].

3.1. Derivation of ΔP - $\Delta\delta$ Relation

The ΔP - $\Delta\delta$ relation of a single fiber can be derived as follows. In the case of a single fiber, the opening displacement change, $\Delta\delta$, between the crack planes is attributed to stretching, unstretching, and contracting of the fiber on both sides of the crack line, i.e. the axial strain change of the fiber before and after unloading[5]. When a single fiber is loaded up to a certain load level, P_{max}, for pull-out and is unloaded to a lower load level, P_{min} ($\Delta P = P_{max} - P_{min}$), the crack opening displacement change, $\Delta\delta$, is given by

$$\Delta\delta = \int_0^{L_f} \left(\varepsilon_{max}(x) - \varepsilon_{min}(x)\right)dx \quad (6)$$

where $\varepsilon_{max}(x) =$ axial strain in the fiber at P_{max}, $\varepsilon_{min}(x) =$ axial strain in the fiber at P_{min}, and x is measured from the shorter embedded end of the fiber. The axial strain of the fiber, $\varepsilon(x)$, can be obtained by

$$\varepsilon(x) = F(x)\Big/\left(\pi\left(\frac{d_f}{2}\right)^2 E_f\right) \quad (7)$$

where $F(x)$ = axial force in the fiber. Equilibrium in the direction of fiber axis requires the applied pull-out load, P, be balanced with the sum of interfacial frictional bond strength. Two assumptions are made for the interfacial frictional bond strength: the interfacial frictional bond strength is constant over all the debonded fiber-matrix interface and unloading creates a zone where the interfacial frictional bond strength acts in the reversed direction to resist moving-in of the fiber. With these assumptions, the equilibrium gives a piecewise linear profile for $F(x)$ and also for $\varepsilon(x)$ (movement of the crack surfaces relative to the fiber is assumed to have little effect on the crack opening displacement change).

Fibers are divided into the two groups as in monotonic loading: debonding and sliding. Namely, fibers are in debonding process for those with long embedment length and in sliding process for those with short embedment length in the preceding loading for pull-out. The fiber axial strain arises in the debonded portion inside the matrix and the exposed portion between the crack surfaces, and it equals to zero in the undebonded region. Thus the integration in (6) can be carried out only for the debonded and exposed portion of the fiber. The details of derivation are shown elsewhere[3]. See also Appendix 1.

For fibers that have been in debonding stage under the preceding pull-out loading, we have

$$\Delta P_1(\Delta\delta) = \pi\sqrt{\frac{\pi d_f^3 E_f \Delta\delta}{2}}, \qquad (8)$$

and for fibers that have been in sliding stage under the preceding pull-out loading,

$$\Delta P_2(\Delta\delta) = -\frac{3}{2}(P_o - P_{\max})$$
$$+ \sqrt{\frac{9}{4}(P_o - P_{\max})^2 + \frac{\pi^2 \pi d_f^3 E_f \Delta\delta}{2}} \qquad (9)$$

where $P_o = \pi \tau d_f l$.

These two equations (8) and (9) also hold for push-in loading ($P_{min} \le 0$). However, for fibers in sliding stage, the crack opening displacement due to the sliding-out induced by the preceding pull-out loading is by orders larger than the crack opening displacement change due to the axial strain change (6). Full crack closure is attained by sliding-in of the entire fiber which follows unstretching and contracting of the fiber (9). The sliding-in takes place at $P_{min} = -P_{max}$ at which the interfacial zone with the reversed frictional bond strength reaches the embedded end of the fiber. For further push-in loading from $-P_{max}$ to $-P_o$, at which the retrieval of the fiber into the matrix is completed, we have

$$\Delta P_3(\Delta\delta) = \pi\tau d_f \Delta\delta + 2P_{\max} - \frac{4P_{\max}}{\pi d_f^2 E_f}(3P_o - P_{\max})$$
$$for\ -P_o \le P_{min} \le -P_{max}. \qquad (10)$$

During the sliding-in, the crack opening displacement change, $\Delta\delta$, is attributed to the sliding-in displacement which is represented by the first term of (10).

The single fiber unloading branches represented by (8)-(10) are illustrated in Fig. 2. Note that $P = P_{max} - \Delta P$ and $\delta = \delta_{max} - \Delta\delta$, given the starting point for unloading (δ_{max}, P_{max}).

4. Fiber Bridging Constitutive Law under Cyclic Loading

4.1. Numerical Solution

The fiber bridging constitutive law under cyclic loading, $\Delta\sigma_f (\Delta\delta)$, that relates the fiber bridging stress amplitude, $\Delta\sigma_f$, and the crack opening displacement amplitude, $\Delta\delta$, can be obtained in the same manner as in monotonic loading, allowing for the random distribution of fiber location and orientation at a designated crack plane. The fiber bridging constitutive law is obtained by

$$\Delta\tilde{\sigma}_f = \frac{8}{\pi\tau(L_f/d_f)d_f^2}$$
$$\int_{\phi=0}^{\frac{\pi}{2}} \int_{z=0}^{\frac{L_f}{2}\cos\phi} \Delta P(\Delta\delta)e^{f\phi}p(\phi)p(z)dzd\phi \qquad (11)$$

where $\Delta\tilde{\sigma}_f = \Delta\sigma_f / \sigma_o$. (8)-(10) are substituted into $\Delta P(\Delta\delta)$ in (11). $\Delta\tilde{\sigma}_f$ is divided into two terms of bridging stress amplitude carried by fibers that have been in debonding and sliding under the preceding monotonic loading:

$$\Delta\tilde{\sigma}_f = \Delta\tilde{\sigma}_f\big|_{debonding} + \Delta\tilde{\sigma}_f\big|_{sliding}. \qquad (12)$$

The first term for fibers that have been in debonding stage can be obtained with the use of (8). Replacing $z / (L_f / 2)$ with z', the integration leads to

$$\Delta\tilde{\sigma}_f\big|_{debonding} = \frac{8}{\pi\tau(L_f/d_f)d_f^2}$$
$$\int_{\phi=0}^{\frac{\pi}{2}} \int_{z'=0}^{z_o\cos\phi} \Delta P_1(\Delta\delta)e^{f\phi} \sin\phi dz' d\phi \qquad (13)$$

$$= g2\sqrt{2}\left(\frac{\Delta\tilde{\delta}}{\tilde{\delta}_{max}}\right)^{\frac{1}{2}} \left(\frac{\tilde{\delta}_{max}}{\tilde{\delta}^*}\right)^{\frac{1}{2}} \left(1 - \left(\frac{\tilde{\delta}_{max}}{\tilde{\delta}^*}\right)^{\frac{1}{2}}\right) \quad (14)$$

where $z_o = 1 - \sqrt{\tilde{\delta}_{max}/\tilde{\delta}^*}$, $\Delta\tilde{\delta} = \Delta\delta/(L_f/2)$, and $\tilde{\delta}_{max} = \delta_{max}/(L_f/2)$.

Similarly the second term for fibers that have been in sliding stage can be obtained with the use of (9) and (10):

$$\Delta \tilde{\sigma}_f \big|_{sliding} = \frac{8}{\pi \tau (L_f / d_f) d_f^2}$$

$$\int_{\phi=0}^{\frac{\pi}{2}(1-\tilde{\delta}_{max})\cos\phi} \int_{z'=z_o \cos\phi} \Delta P_{2or3}(\Delta\delta) e^{f\phi} \sin\phi \, dz' \, d\phi \qquad (15)$$

where

$$\Delta P_{2or3}(\Delta\delta) = the \; smaller \; of \begin{Bmatrix} \Delta P_2(\Delta\delta) \\ \Delta P_3(\Delta\delta) \end{Bmatrix}. \qquad (16)$$

The second term is obtained by numerical integration while choosing the smaller of ΔP_2 and ΔP_3 numerically.

The resulting unloading curves of the bridging stress-crack opening displacement relation are shown in Fig. 3 and 4 together with the curve of the monotonic constitutive law. Note that $\tilde{\sigma}_f = \tilde{\sigma}_{f max} - \Delta \tilde{\sigma}_f$ and $\tilde{\delta} = \tilde{\delta}_{max} - \Delta\tilde{\delta}$, given the starting point for unloading ($\tilde{\delta}_{max}$, $\tilde{\sigma}_{f max}$). Fig. 3 for the pre-peak part shows that some remaining crack opening displacement exists even after full unloading to zero and that further compressive loading is required to attain full crack closure. Fig. 4 for the post-peak part shows that the crack opening displacement change is given initially by unstretching and contracting of the fibers, followed by sliding-in of the fibers.

Examinations of a crack after tests needs the analysis of cyclic fiber bridging behavior, especially for crack width measurement. A crack tends to close, when the fiber bridging stress is decreased upon overall unloading of a cracked fiber composite, but the crack usually has some remaining opening displacement due to the incomplete retrieval of the bridging fibers into the matrix, thus the crack being visible. The theoretical results qualitatively confirm the typical behavior of DFRCs under cyclic loading.

4.2. Approximate Analytical Solution

The numerical evaluation of the cyclic fiber bridging constitutive law is time-consuming, particularly when the constitutive law is implemented into a numerical code which solves a fatigue crack growth problem via iterations[6][7][8]. The constitutive law is obtained also in an analytical form by approximating the ΔP - $\Delta\delta$ relation.

For fibers that have been in debonding stage under the preceding pull-out loading, we have the same ΔP - $\Delta\delta$ relation:

$$\Delta P_1(\Delta\delta) = \pi \sqrt{\frac{\tau d_f^3 E_f \Delta\delta}{2}}, \qquad (17)$$

and for fibers that have been in sliding stage under the preceding

pull-out loading, we assume that the ΔP - $\Delta\delta$ relation is the same as that for fibers that have been in debonding. Namely, the fibers undergo unstretching and contracting according to

$$\Delta P_2(\Delta\delta) = \Delta P_1(\Delta\delta) = \pi \sqrt{\frac{\tau d_f^3 E_f \Delta\delta}{2}}. \qquad (18)$$

Furthermore, when these fibers slide back into the matrix after unstretching and contracting, we assume that the ΔP - $\Delta\delta$ relation is given by

$$\Delta P_3(\Delta\delta, \delta_{max}) = \pi \tau d_f \Delta\delta + 2 P_{max} \qquad (19)$$

where $P_{max} = \pi \tau d_f (l - \delta_{max})$. This approximation is based on a physical assumption that the fiber strain change between the crack surfaces does not contribute to the crack opening displacement change, $\Delta\delta$, while the fiber strain change in the debonded region inside the matrix does.

The constitutive law derived with the approximate ΔP - $\Delta\delta$ relation can be represented by analytical equations, and details can be found in Appendix 2. The resulting constitutive law, $\Delta\sigma_f$ ($\Delta\delta$), is given in a normalized form by

$$\Delta\tilde{\sigma}_f = \begin{cases} \Delta\tilde{\sigma}_f \big|_{prepeak} & (for \; 0 \le \tilde{\delta}_{max} \le \tilde{\delta}^*) \\ \Delta\tilde{\sigma}_f \big|_{postpeak} & (for \; \tilde{\delta}^* < \tilde{\delta}_{max} \le 1) \end{cases}. \qquad (20)$$

For pre-peak part, we have

$$\Delta\tilde{\sigma}_f \big|_{prepeak} = g \left[2\sqrt{2} \left(\frac{\Delta\tilde{\delta}}{\tilde{\delta}^*} \right)^{\frac{1}{2}} (1 - \tilde{\delta}_{max}) - \frac{\Delta\tilde{\delta}}{\tilde{\delta}^*} \right.$$

$$\left. + \sqrt{2} \left(\frac{\Delta\tilde{\delta}}{\tilde{\delta}^*} \right)^{\frac{3}{2}} \tilde{\delta}^* - \frac{1}{2} (\Delta\tilde{\delta})^2 \right]. \qquad (21)$$

For post-peak part, there are two stages. When only some fibers are in sliding back into matrix and other fibers are in unstretching and contracting ($\beta \le \beta_o$), the constitutive law is the same as that of the pre-peak part and is given by

$$\Delta\tilde{\sigma}_f \big|_{postpeak} (\beta \le \beta_o) = g \left[2\sqrt{2} \left(\frac{\Delta\tilde{\delta}}{\tilde{\delta}^*} \right)^{\frac{1}{2}} (1 - \tilde{\delta}_{max}) \right.$$

$$\left. - \frac{\Delta\tilde{\delta}}{\tilde{\delta}^*} + \sqrt{2} \left(\frac{\Delta\tilde{\delta}}{\tilde{\delta}^*} \right)^{\frac{3}{2}} \tilde{\delta}^* - \frac{1}{2} (\Delta\tilde{\delta})^2 \right] \qquad (22)$$

where $\beta = \Delta\tilde{\delta} / \tilde{\delta}_{max}$ and

$$\beta_o = \left(\frac{\sqrt{\dfrac{\tilde{\delta}_{max}}{2\tilde{\delta}^*}} - \sqrt{\dfrac{\tilde{\delta}_{max}}{2\tilde{\delta}^*} - 2\tilde{\delta}_{max}\left(1 - \tilde{\delta}_{max}\right)}}{\tilde{\delta}_{max}} \right)^2 . \quad (23)$$

When all fibers are in sliding back into matrix $(\beta_o < \beta)$, the constitutive law is given by

$$\Delta\tilde{\sigma}_f\big|_{postpeak} \left(\beta_o < \beta\right) = g\left[2\left(1 - \tilde{\delta}_{max}\right)\left(1 - \tilde{\delta}_{max} + \Delta\tilde{\delta}\right)\right] . \quad (24)$$

This approximate constitutive law is compared with the numerical one of the previous section. Two fiber types (polyethylene and polypropylene fiber) are examined for various values of the crack opening displacement at maximum load level, δ_{max}, and the crack opening displacement amplitude, $\Delta\delta$. The relation between bridging stress and crack opening displacement is shown in Fig. 5 and Fig. 6 in a normalized form, where $\alpha = \tilde{\delta}_{max}/\tilde{\delta}^*$ and $\beta = \Delta\tilde{\delta}/\tilde{\delta}_{max}$. The fiber composite system parameter, $\tilde{\delta}^* = (2 \tau L_f)/(E_f d_f)$, is 0.0028 for polyethylene ($\tau = $ 0.5 MPa, $L_f = 12.7$ mm, $E_f = 120$ GPa, and $d_f = 38$ μm) and 0.033 for polypropylene ($\tau = 0.8$ MPa, $L_f = 12$ mm, $E_f = 12$ GPa, and $d_f = 48$ μm). The normalized bridging stress, $\Delta\sigma_f / \sigma_o$, in Fig. 5 and Fig. 6 takes the maximum value at $\alpha = \alpha_o$ which gives $\beta_o = 1$ in (23). α_o is 1.98 for polyethylene, and 1.87 for polypropylene. The main difference between the two fiber types is the elastic modulus, namely the elastic modulus of polyethylene is one order stiffer than that of polypropylene.

The difference between the analytical solution and the numerical one is negligible for polyethylene fiber, while the difference is noticeable for polypropylene fiber especially for the cases of large α's. This is because of the lower elastic modulus of polypropylene fiber. Lower elastic modulus contributes more to crack opening displacement change via axial fiber strain change between crack surfaces, but this contribution is ignored according to the aforementioned assumption. Therefore, the stiffer polyethylene fiber shows negligible difference, while the more compliant polypropylene shows a noticeable difference, especially for large crack opening displacement cases (large α's) where more portion of fibers are exposed between crack surfaces.

However, even in the case of polypropylene fiber, the difference is not significant for small α's which are usually experienced in fatigue crack growth computations, and, of course, the approximate solution can replace the numerical one in the case of polyethylene fiber.

5. Validation of the Cyclic Fiber Bridging Constitutive Law

The theoretical cyclic bridging constitutive law derived in the previous section is compared with experimental data of uniaxial
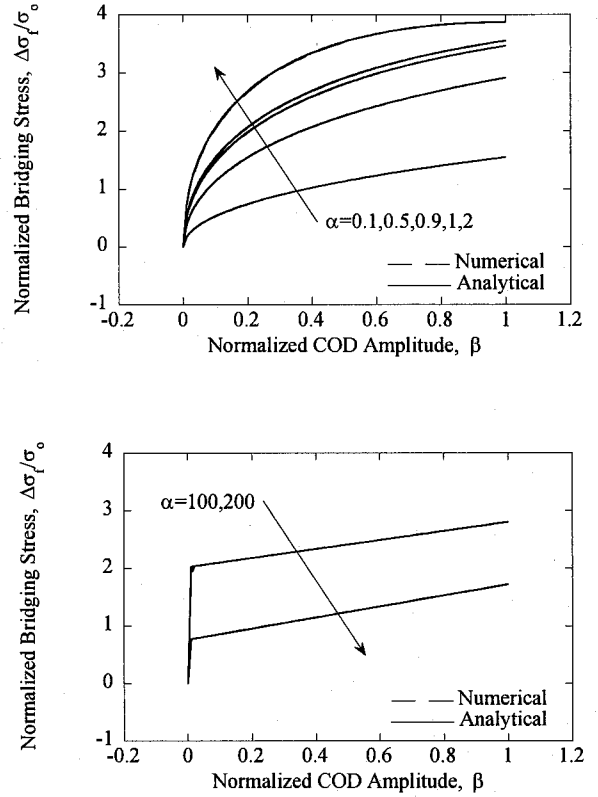

Fig. 5 Comparison between numerical and analytical solution (polyethylene fiber $\tilde{\delta}^* = 0.0028$).
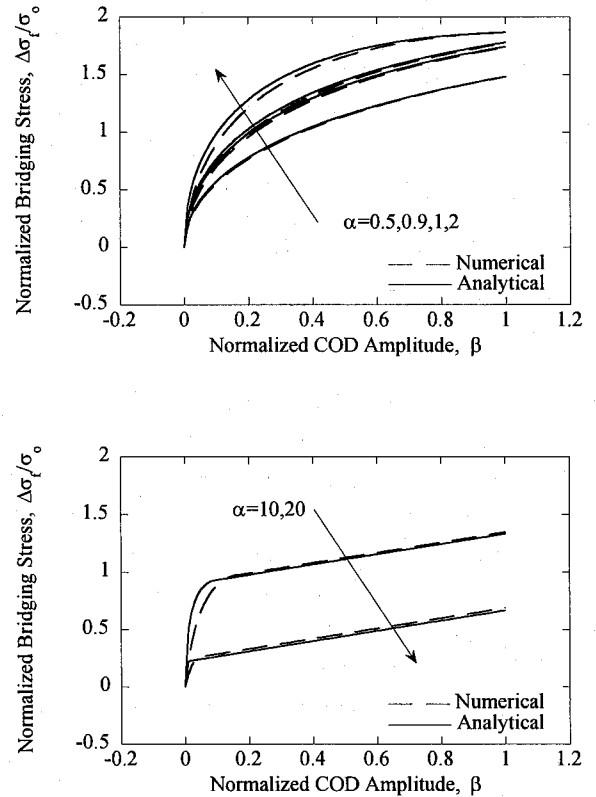

Fig. 6 Comparison between numerical and analytical solution (polypropylene fiber $\tilde{\delta}^* = 0.033$)

- 928 -

cyclic response of an FRC which is reported by Zhang et al[9]. The comparison shows a good agreement, supporting the validity of the theoretical cyclic bridging constitutive law.

The cyclic loading test of an FRC is briefly summarized here. The tested FRC contains coarse aggregates of 8 mm maximum and is reinforced with 1 vol. % of smooth steel fiber (see Table 1 for fiber parameters). The FRC specimen has dimensions of height 55 mm, width 60 mm, and thickness 50 mm, and its two sides have a notch of 9 mm depth and 3 mm width. The specimen was loaded in uniaxial tensile load and unloaded at eight preset displacement values: 0.01, 0.03, 0.05, 0.1, 0.2, 0.3, 0.4, and 0.5 mm. Deformation over the notch of each side was measured by extensometers with the gauge length of 12.5 mm. Fig. 7 shows the measured relation between the applied stress and the gauge displacement under the aforementioned loading sequence. In the experimental measurement, steep hysteresis loops with some remaining displacement at zero load level are observed, therefore the crack does not close even after full unloading. This is a common observation in the cyclic response of FRCs[10]. The width of hysteresis loops changes from one to another, and it is the widest for the unloading-reloading branch from 0.2 mm.

From this particular plot, the tensile strength is 4.1 MPa, and the composite modulus is 7.3 GPa, while they are reported to be 5.42 MPa and 35 GPa based on direct tensile and compressive tests respectively. The measured composite modulus of 7.3 GPa is apparently very low, and this is due to the notches made on the sides of the specimen. Also lower modulus in tension than compression in fiber reinforced cementitious materials has been measured[11]. In this comparison, the composite modulus

Table 1 Fiber parameters[9].

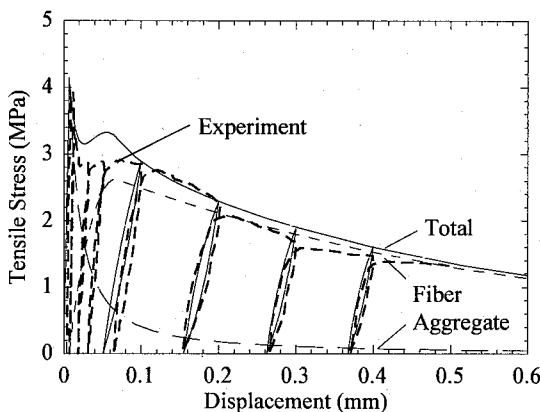| Type	L_f(mm)	E_f(GPa)	d_f(μm)	V_f(%)
smooth steel	25	210	400	1

Fig. 7 Experimental curve of cyclic response[9] and theoretical curves of cyclic response of a steel FRC.

of 7.3 GPa is used throughout for an input parameter to theoretical constitutive laws, including unloading and reloading branches in the cyclic response of the FRC (see Table 2 for matrix parameters).

Crack bridging stress of the FRC has to be evaluated, since it is assumed that the FRC is deformed elastically up to the peak, then it is cracked at the peak, thus activating bridging stress across the crack. Crack bridging stress of the FRC is exerted by aggregates and fibers, and it is assumed that the crack bridging stress is obtained by the superposition of these two bridging stresses. The aggregate bridging stress under monotonic loading is given by an empirical equation proposed by Stang[12]. The aggregate bridging stress, σ_m, as a function of the crack opening displacement, δ, is given by

$$\sigma_m(\delta) = \frac{\sigma_m^u}{1 + \left(\dfrac{\delta}{\delta_{mo}}\right)^p} \qquad (25)$$

where σ_m^u = maximum aggregate bridging stress at $\delta = 0$, δ_{mo} = crack opening displacement which corresponds to the half of σ_m^u, and p describes the shape of the bridging curve. The aggregate bridging stress under cyclic loading is given by

$$\Delta\sigma_m(\Delta\delta) = \frac{\sigma_{m\max}}{\delta_{\max} - \delta_{\min}}\Delta\delta \qquad (26)$$

where ($\delta_{\max}$, $\sigma_{m\max}$) is the point at which unloading occurs and ($\delta_{\min}$, 0) is the point at which the FRC is fully unloaded to zero load level. These two points are taken from the experimental plot for each unloading-reloading branch. The fiber bridging stress under monotonic loading is obtained with (4) and (5), while that under cyclic loading is obtained with (21), (22), and (24).

Theoretical relation between tensile stress and displacement for the FRC can be obtained as follows. The theoretical curves are obtained in the following three regions: up to the peak stress, after the peak stress, and in the hysteresis loops. First, in the region up to the peak stress, the displacement is attributed to the elastic deformation within the gauge length, since no crack is assumed before the peak stress is reached. The composite modulus of 7.3 GPa that is obtained from the plot and the gauge length are used to calculate the response of the FRC. Second, in the region after the peak stress, a crack is assumed to be formed and bridged by aggregates and fibers. Therefore, the

Table 2 Matrix parameters[9].

E_m (GPa)	σ_m^u (MPa)	p	δ_{mo} (mm)
35 (7.3 from the plot)	5.42 (4.1 from the plot)	1.2	0.015

displacement is attributed to both of elastic deformation and crack opening displacement within the gauge. The crack bridging stress decreases, as the crack opens up, and accordingly the elastic deformation within the gauge length decreases. In the fiber bridging stress, slip softening relation at the fiber-matrix interface under monotonic loading is assumed. The relation is given by

$$\tau_{mono}(\delta) = \begin{cases} \tau_o & for \ \delta \leq \delta^* \\ \tau_o + a_1\delta + a_2\delta^2 & for \ \delta^* < \delta \end{cases} \quad (27)$$

where τ_o = initial bond strength and a_1, a_2 = coefficient, and it accounts for frictional wearing at the interface. Also the Cook-Gordon effect is included[13)14)]. Third, in the hysteresis loops, the displacement change is attributed still to both of elastic deformation and crack opening displacement within the gauge length, but the unloading and reloading of aggregates and fibers follow the cyclic bridging constitutive laws shown above. Unloading and reloading of aggregate bridging show the linear elastic response as described in (26). Unloading path of fiber bridging is determined by subtracting the changes ($\Delta\delta$, $\Delta\sigma_f$) from the coordinates at which unloading take place (δ_{max}, σ_f), and reloading path is determined by adding the changes to the coordinates at which reloading takes place (δ_{min}, σ_f). Theoretical curves of cyclic response of the FRC are shown in Fig. 7 together with experimental curves in the same figure. The cyclic response of the FRC is successfully reproduced by the theoretical curves. The stiffness of the hyteresis loops agrees with the experimental one, and the loops have some remaining crack opening displacement at zero load level. Furthermore, the width of hysteresis loops shows the same trend, namely it is the largest at 0.2 mm

From the comparison, the interfacial frictional bond strength, τ_o, and the coefficients, a_1 and a_2, are deduced. The set of these parameters shown in Table 3 and Table 4 yields a close agreement with the experimental curves. The deduced values in Table 3 for monotonic loading fall within reported values[15)], whereas, for cyclic loading, it is found that the interfacial frictional bond strength under cyclic loading is lower than that

Table 3 Maximum and minimum opening displacement[9)] and estimated interfacial bond strength at each of hysteresis loops.

δ_{max} (mm)	0.1	0.2	0.3	0.4
δ_{min} (mm)	0.063	0.151	0.263	0.37
τ_{mono} (MPa)	4.2	3.6	3.1	2.7
τ_{cyc} (MPa)	4.2 ×0.6	3.6 ×0.6	3.1 ×0.6	2.7 ×0.6

Table 4 Interface parameters for fatigue hysteresis loops[9)].

τ_{mono} (MPa)	τ_{cyc} (MPa)	f
6.0	6.0 × 0.6	0.8

under monotonic loading and that $\tau_{cyc} = 0.6 \ \tau_{mono}$ yields the best fit to the experimental hysteresis loops. This apparently lower frictional bond strength under cyclic loading is presumably because the normal pressure acting on the fiber is reduced near the crack surface as the surrounding matrix is destressed with the fiber pullout, when compared to around the embedded fiber end. This reduced normal pressure leads to the lower Coulomb frictional shear stress in the reversed frictional area near the crack surfaces, which suggests that the interfacial frictional bond strength is not constant along the interface of an embedded fiber as opposed to a model assumption and lowest near the crack surfaces.

It is shown that the theoretical fiber bridging constitutive laws under cyclic loading successfully reproduces the cyclic response of an FRC in terms of the stiffness and width of the hysteresis loops and that the interfacial frictional bond strength under cyclic loading is lower than that under monotonic loading presumably due to the destressed surrounding matrix in the reversed frictional area.

Although the developed $\Delta\sigma_f$ - $\Delta\delta$ relation has been validated with the experimentally obtained cyclic responses of an FRC, the developed ΔP - $\Delta\delta$ relation can also be utilized to understand single fiber pull-out behaviors. This differentiates the current approach from others, since the effects of each of microparameters on $\Delta\sigma_f$ - $\Delta\delta$ relation can be evaluated explicitly.

6. Concluding Remarks

This paper presents a theoretical formulation of the cyclic constitutive law for discontinuous fiber reinforced composites (DFRCs). The formulation is based on the micromechanics of fiber bridging under cyclic loading, enabling the effects of microstructural parameters to be evaluated.

The single fiber pull-out/push-in load amplitude-crack opening displacement amplitude relation (ΔP - $\Delta\delta$ relation) is derived assuming that the fiber-matrix interface is friction-controlled.

The fiber bridging constitutive law under cyclic loading ($\Delta\sigma_f$ - $\Delta\delta$) is derived numerically and analytically by integrating the load carried by individual fibers according to the ΔP - $\Delta\delta$ relation. The theoretical constitutive law is compared with experimental data of an FRC under cyclic loading and agrees well. It is shown that the theoretical fiber bridging constitutive laws under cyclic loading successfully reproduces the cyclic response of the FRC in terms of the stiffness and width of the hysteresis loops and that the interfacial frictional bond strength under cyclic loading is 40% lower than that under monotonic loading presumably due to destressed surrounding matrix in the reversed frictional area.

With the use of the developed bridging constitutive law under cyclic loading, it is possible to analyze fatigue crack growth in

discontinuous fiber reinforced composites. Fatigue crack growth can be described with Paris law, where fatigue crack growth rate is expressed in terms of stress intensity factor amplitude, ΔK_{tip}. In the case of discontinuous fiber reinforced composites, ΔK_{tip} is related not only to applied stress, $\Delta\sigma_a$, but also to fiber bridging stress, $\Delta\sigma_f$. And, it is necessary to have an explicit $\Delta\sigma_f$ - $\Delta\delta$ relation for varying maximum crack opening displacement, δ_{max}, during fatigue crack propagation. The current $\Delta\sigma_f$ - $\Delta\delta$ relation meets this requirement. The fatigue life of discontinuous fiber reinforced composites can then be described in terms of microstructural parameters, which is beneficial for understanding fatigue mechanism and improving fatigue durability.

Appendix 1 Derivation of the relation between fiber pull-out load amplitude and crack opening displacement amplitude

The integration in (6) leads to the following results. For fibers that have been in debonding stage under the preceding pull-out loading, we have

$$\Delta\delta = \frac{2(\Delta P)^2}{\pi^2 \tau d_f^3 E_f}, \tag{A1}$$

and, for fibers that have been in sliding stage under the preceding pull-out loading,

$$\Delta\delta = \frac{1}{\pi^2 \tau d_f^3 E_f}\left(2(\Delta P)^2 + 6\Delta P(P_o - P_{max})\right) \tag{A2}$$

where P_o = pullout load at which debonding is completed. These two equations (A1) and (A2) also hold for compressive loading ($P_{min} \leq 0$). However, fibers that have been in sliding stage start sliding into matrix when $P_{min} = -P_{max}$. Hence, for further push-in loading from $-P_{max}$ to $-P_o$ at which the retrieval of the fiber into the matrix is completed, we have

$$\Delta\delta = \frac{\Delta P - 2P_{max}}{\pi \tau d_f} + \frac{1}{\pi^2 \tau d_f^3 E_f}\left(12 P_{max} P_o - 4 P_{max}^2\right)$$

$$for -P_o \leq P_{min} \leq -P_{max} \tag{A3}$$

During the sliding-in of fibers, $\Delta\delta$ is attributed mainly to sliding distance, which is represented by the first term of (A3), under constant interfacial frictional stress. These three equations reduce to the form of (8), (9), and (10).

Appendix 2 Derivation of the approximate fiber bridging constitutive law under cyclic loading

It is assumed that fibers are randomly distributed in a fiber composite for the fiber centroidal distance, z, and orientation, ϕ, at a designated crack plane (Fig. 1 for angle and centroidal distance). Under monotonic loading, these bridging fibers can be divided into two groups (Fig. A1). The first group includes the fibers that are still undergoing debonding at the fiber-matrix interface, and the second group includes the fibers that have completed debonding and are sliding out of the matrix. These two groups of fibers contribute to the fiber bridging stress. In addition to these two groups of fibers, there are fibers that have been pulled out of the matrix, but these fibers do not contribute to the bridging stress.

A fiber with its embedment length, l, is still in debonding process and belongs to the first group, if the current crack opening displacement, δ, is smaller than $\delta_o = (4 \tau l^2) / (E_f d_f)$, which is the crack opening displacement at complete debonding. This is given by

$$\delta < \delta_o = \frac{4\tau l^2}{E_f d_f} = \frac{4\tau}{E_f d_f}\left(\frac{L_f}{2} - \frac{z}{\cos\phi}\right)^2 \tag{A4}$$

where τ = interfacial frictional bond strength, E_f = fiber modulus, d_f = fiber diameter, and L_f = fiber length. With $z' = z / (L_f / 2)$, this becomes

$$z' < \left[1 - \sqrt{\frac{\tilde{\delta}_{max}}{\tilde{\delta}^*}}\right]\cos\phi = z_o \cos\phi \tag{A5}$$

where $\tilde{\delta}_{max} = \delta_{max} / (L_f / 2)$, δ_{max} = maximum crack opening displacement in a load cycle, $\tilde{\delta}^* = (2 \tau L_f) / (E_f d_f)$, and this means that fibers in the domain of $\{(w = z' /\cos\phi, \phi)| 0 < w < z_o, 0 < \phi < \pi / 2\}$ are in debonding process (Fig. A1). Similarly, a fiber is in sliding-out process and belongs to the second group, if δ is larger than δ_o and smaller than l:

$$\delta_o < \delta < l = \frac{L_f}{2} - \frac{z}{\cos\phi} \tag{A6}$$

or

$$z_o \cos\phi < z' < (1 - \tilde{\delta}_{max})\cos\phi. \tag{A7}$$

This means that fibers in the domain of $\{(w, \phi)| z_o < w < 1 - \tilde{\delta}_{max}, 0 < \phi < \pi / 2\}$ are in sliding-out process (Fig. A1). The upper limit on z' ensures that the fibers already pulled out do not contribute to the bridging stress.

Under cyclic loading, the single fiber behavior is dependent on the previous monotonic loading. The first group of fibers

undergoes unstretching and contracting upon unloading, so the bridging stress arising from this group can be obtained by the integration of the contribution of individual fibers, $\Delta P_1(\Delta\delta)$ which is given by (17), in the domain $\{(w, \phi)| 0 < w < z_o, 0 < \phi < \pi/2\}$. The second group of fibers is further divided. The fibers that have been in sliding-out process undergo sliding-in subsequent to unstretching and contracting. The sliding-in of a fiber takes place when $\Delta P_2 > \Delta P_3$. This condition can be solved with the approximation of the ΔP - $\Delta\delta$ relation: (18) and (19). It is given by

$$z' > \left[\frac{\Delta\tilde{\delta}}{2} + 1 - \tilde{\delta}_{max} - \sqrt{\frac{\Delta\tilde{\delta}}{2\tilde{\delta}^*}}\right]\cos\phi = z_1\cos\phi. \quad (A8)$$

where $\Delta\tilde{\delta} = \Delta\delta/(L_f/2)$. In the second group, the bridging stress arising from the fibers that are in unstretching and contracting can be obtained by the integration of the contribution of individual fibers, $\Delta P_2(\Delta\delta)$ which is given by (18), in the domain $\{(w, \phi)| z_o < w < z_1, 0 < \phi < \pi/2\}$. And the bridging stress arising from the fibers in sliding-in can be obtained by the integration of $\Delta P_3(\Delta\delta)$ given by (19) in the domain $\{(w, \phi)| z_1 < w < 1 - \tilde{\delta}_{max}, 0 < \phi < \pi/2\}$.

When cyclic loading takes place from a point of the pre-peak bridging curve ($0 \le \tilde{\delta}_{max} \le \tilde{\delta}^*$), the bridging stress is carried by both of the first and second group of fibers. We have the contribution of $\Delta P_1(\Delta\delta)$, $\Delta P_2(\Delta\delta)$, and $\Delta P_3(\Delta\delta)$:

$$\Delta\tilde{\sigma}_f\Big|_{prepeak} = \frac{8}{\pi\tau(L_f/d_f)d_f^2}$$

$$\left\{ \int_{\phi=0}^{\frac{\pi}{2}}\int_{z'=0}^{z_o\cos\phi}\Delta P_1(\Delta\delta)e^{f\phi}\sin\phi dz'd\phi \right.$$

$$(A9)$$

$$+ \int_{\phi=0}^{\frac{\pi}{2}}\int_{z'=z_o\cos\phi}^{z_1\cos\phi}\Delta P_2(\Delta\delta)e^{f\phi}\sin\phi dz'd\phi$$

$$\left. + \int_{\phi=0}^{\frac{\pi}{2}}\int_{z'=z_1\cos\phi}^{(1-\tilde{\delta}_{max})\cos\phi}\Delta P_3(\Delta\delta)e^{f\phi}\sin\phi dz'd\phi \right\},$$

and this reduces to the form in (21).

When cyclic loading takes place from a point of the post-peak bridging curve ($\tilde{\delta}^* < \tilde{\delta}_{max} \le 1$), the bridging stress is carried by the second group of fibers only. This is because all fibers have completed debonding at the peak bridging stress, and no fibers of the first group exists. For a small COD amplitude ($\beta \le \beta_o$), there are fibers in unstretching and contracting and in sliding-in. Hence, we have the contribution of $\Delta P_2(\Delta\delta)$ and $\Delta P_3(\Delta\delta)$:

$$\Delta\tilde{\sigma}_f\Big|_{postpeak} (\beta \le \beta_o)$$

$$= \frac{8}{\pi\tau(L_f/d_f)d_f^2}\left\{ \int_{\phi=0}^{\frac{\pi}{2}}\int_{z'=0}^{z_1\cos\phi}\Delta P_2(\Delta\delta)e^{f\phi}\sin\phi dz'd\phi \right. \quad (A10)$$

$$\left. + \int_{\phi=0}^{\frac{\pi}{2}}\int_{z'=z_1\cos\phi}^{(1-\tilde{\delta}_{max})\cos\phi}\Delta P_3(\Delta\delta)e^{f\phi}\sin\phi dz'd\phi \right\},$$

and we obtain (22). For a large COD amplitude ($\beta_o < \beta$), all fibers are in sliding-in, and we only have the contribution of $\Delta P_3(\Delta\delta)$:

$$\Delta\tilde{\sigma}_f\Big|_{postpeak} (\beta_o < \beta)$$

$$= \frac{8}{\pi\tau(L_f/d_f)d_f^2}\left\{ \int_{\phi=0}^{\frac{\pi}{2}}\int_{z'=0}^{(1-\tilde{\delta}_{max})\cos\phi}\Delta P_3(\Delta\delta)e^{f\phi}\sin\phi dz'd\phi \right\}, \quad (A11)$$
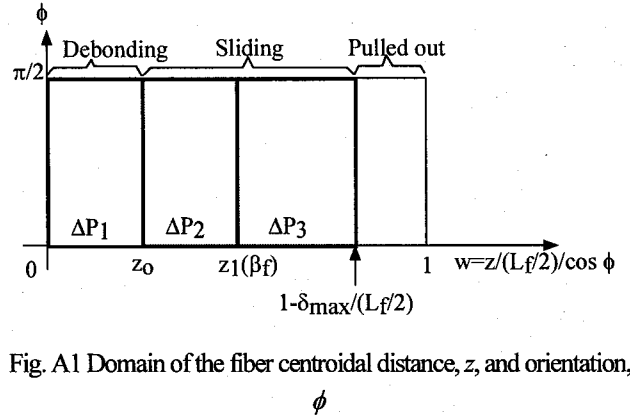
and we obtain (24).

Fig. A1 Domain of the fiber centroidal distance, z, and orientation, ϕ

References

1) Li, V. C., Postcrack Scaling Relations for Fiber Reinforced Cementitious Composites, *Journal of Materials in Civil Engineering*, 4(1), 41-57, 1992.

2) Li, V. C. and Leung, C. K. Y., Steady State and Multiple Cracking of Short Random Fiber Composites, *Journal of Engineering Mechanics*, 188(11), 2246-2264, 1992.

3) Matsumoto, T. and Li, V. C., Uniaxial Cyclic Behavior of Discontinuous Fiber Reinforced Composites. *Proc. ASCE 4th Materials Engineering Conference*, Washington D.C., USA, 426-435, 1996.

4) Li, V. C., Wang, Y., and Backer, S., Effect of Inclining Angle, Bundling, and Surface Treatment on Synthetic Fiber Pull-Out from a Cement Matrix, *Journal of Composites*, 21(2), 132-140. 1990.

5) McMeeking, R. M. and Evans, A. G., Matrix Fatigue

Cracking in Fiber Composites, *Mechanics of Materials*, 9, 217-227, 1990.

6) Li, V. C. and Matsumoto, T., Fatigue Crack Growth Analysis of Fiber Reinforced Concrete with Effect of Interfacial Bond Degradation, *Journal of Cement and Concrete Composites*, 20(5), 339-351, 1998.

7) Matsumoto, T. and Li, V. C., Fatigue Crack Fracture and Arrest in Fiber Reinforced Concrete under Interfacial Bond Degradation, *Fracture Mechanics of Concrete Structures (FRAMCOS-3)*, Gifu, Japan, 541-550, 1998.

8) Matsumoto, T. and Li, V. C., Fatigue Life Analysis of Fiber Reinforced Concrete with a Fracture Mechanics Based Model, *Journal of Cement and Concrete Composites*, 21(4), 249-261, 1999.

9) Zhang, J., Stang, H., and Li, V. C., Experimental Study on Crack Bridging in FRC under Uniaxial Fatigue Tension, *Journal of Materials in Civil Engineering*, 12(1), 66-73, 2000.

10) Gopalaratnam, V. S. and Shah, S. P., Tensile Failure of Steel Fiber-Reinforced Mortar, *Journal of Engineering Mechanics*, 113(5), 635-652. 1987.

11) Mishra, D., Performance of Engineered Cementitious Composites Under Shear Load, *Doctoral Thesis*, The University of Michigan, Ann Arbor. 1995.

12) Stang, H., Evaluation of Properties of Cementitious Fiber Composite Materials, *International RILEM/ACI Workshop, High Performance Fiber Cement Composites*, 388-406, 1992.

13) Cook, J. and Gordon, J. E., A Mechanism for the Control of Crack Propagation in All Brittle Systems, *Proceedings of the Royal Society of London*, A282, 508-520. 1964.

14) Li, V. C., Stang, H., and Krenchel, H., Micromechanics of Crack Bridging in Fiber Reinforced Concrete, *Materials and Structures*, 26, 486-494. 1993.

15) Li, V. C. and Stang, H., Interface Property Characterization and Strengthening Mechanisms in Fiber Reinforced Cement Based Composites, *Journal of Advanced Cement Based Materials*, 6(1), 1-20, 1997.